THE JOURNAL OF PHYSICAL CHEMISTRY A

Article

Cite This: J. Phys. Chem. A 2017, 121, 9708−9719

pubs.acs.org/JPCA

Electronic Properties and Electroluminescent OLED Performance of Panchromatic Emissive *N*-Aryl-2,3-naphthalimides

Lili Bao, Yan Zou, Allison Kirk, and Michael D. Heagy*

Department of Chemistry, New Mexico Institute of Mining & Technology, Socorro, New Mexico 87801, United States

Supporting Information

ABSTRACT: This report investigates the excited-state properties of a series of *N*-aryl-2,3-naphthalimides along with their fabrication into OLEDs and electroluminescence measurements. The *N*-aryl-2,3-NIs substituted specifically with chloro, fluoro, and methoxy substituents were chosen because of their unique propensity to display two emission bands or panchromatic fluorescence. Using the Lippert−Mataga analysis along with TD-DFT calculations, the excited states were determined to be n,π^* and π,π^*. The TD-DFT calculations on the geometries of the excited states indicate that the excited state shows a planar structure. The origin of both the short wavelength (SW) and long wavelength (LW) emission were correlated to specific geometries such that the SW emission originates from an "angled" structure in the excited state, and LW emission originates from an excited state of coplanar structure. All of the dyes investigated readily formed good films under ultrahigh vacuum deposition. The molecular energy levels of these compounds (HOMO and LUMO) were measured with cyclic voltammetry. Band gaps were also measured in both electrochemical and optical methods and indicate that the HOMOs of these fluorophores matched well with the anode (ITO work function), and their LUMOs matched well with the cathode (LiF/Al). To compare photoluminescence of the four dyes with their potential electroluminescence, three OLED devices were designed and fabricated. The electroluminescent spectra of these devices indicate that the panchromatic fluorescence, observed in solution, shifts toward the red in the solid-state. A plausible explanation appears to stem from an inability to inject electrons to the higher LUMO+1 orbitals; a process observed in the solution phase. Hence, the short wavelength fluorescence peak, a key component to panchromatic luminescence disappears in the OLED device. The observed EL spectrum from these smaller heteroatomic architectures is on par if not more broadly emissive than rubrene (5,6,11,12-tetraphenyltetracene), a red-colored $C_{42}H_{28}$ polycyclic aromatic hydrocarbon, that displays an orange-color EL

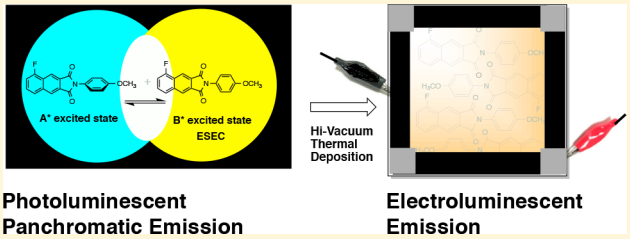

INTRODUCTION

Naphthalimides (NIs) have received considerable attention for both their unique spectroscopic properties and their potential biological applications.[1−6] For instance, NIs have been investigated in site-specific DNA cleavage,[7,8] photodynamic therapy,[9] inducing photo-cross-linking of proteins,[10] and light-induced tissue repair.[11] The charge-transfer (CT) characteristics of NI excited states have also been studied in organic materials, such as donor−acceptor systems for solar cells,[12] organic light-emitting diodes (OLEDs),[13] sensors for metal ions and protons,[14−18] and potential optical switches operating in the picosecond time scale.[19] Interestingly, when the imide nitrogen is substituted by arenes, NIs can be designed to display dual-fluorescence and in certain cases panchromatic emission.[6,20,21] To date, NIs hold the unique advantage of emitting white light with the smallest molecular architecture among so-called single-emitter dyes.[3] This combination of characteristics is highly desirable, since low molecular weight dyes represent low temperature deposition possibilities and facile fabrication techniques.

To follow the evolution of monofluorescent dyes to dual fluorescent to panchromatic, requires an understanding of their excited states. Dual fluorescent molecules have been generally categorized as either tautomeric systems such as excited-state proton transfer (ESPT) or the well-established charge-transfer mechanisms such as intramolecular charge-transfer (ICT) and twisted intramolecular charge-transfer (TICT).[2,21] Because of the rotational dynamics between the *C*-aryl-*N*-imide linkage, *N*-aryl-2,3-naphthalimides may be expected to exhibit TICT excited state characteristics. Instead, Berces et al. in their pivotal publications, concluded that both short wavelength emission (SW) and long wavelength emission (LW) excited states originated from a common Franck−Condon state whereupon subsequent relaxation and emission of the SW originated from an orthogonal structure and LW emission resulted from a coplanar structure.[22−24] These studies concluded that the photophysical mechanism for the dual-fluorescent NIs was neither ESPT nor TICT. Further spectroscopic investigations of 1,8-NIs demonstrated that two emitting states S_1 and S_2 were responsible for SW and LW fluorescence[25−30]

This remarkable luminescent feature from such a small molecular architecture results from a complex interplay of

Received: August 15, 2017
Revised: November 18, 2017
Published: November 28, 2017

DOI: 10.1021/acs.jpca.7b08110
J. Phys. Chem. A 2017, 121, 9708−9719

excited states and subsequent optical changes via appropriately placed substituents at either the naphthalic ring or the *N*-aryl group. Applications of two-color emission, as well as panchromatic fluorescence by NI's, have been reported by our group with examples of ratiometric probes and white-light photoluminescence.[1] The excited state properties of 4-substituted naphthalimides have been recently investigated for their charge-transfer states and single-band emission,[4] however, the excited state properties of dual-fluorescent *N*-aryl-2,3-naphthalimides have not received a similar photophysical investigation. With an eye toward the next generation of OLED technology; specifically WOLEDs, this exploration of NIs aims toward promoting both SW and LW emission to yield not just dual fluorescence but rather panchromatic emission. NIs belong to a class of chromophores where spectroscopic and photophysical properties can be readily changed through (1) the position of the dicarboximide attached to the naphthalene ring, such as 1,2-NI, 2,3-NI, or 1,8-NI[22,29,31] shown in Figure 1,

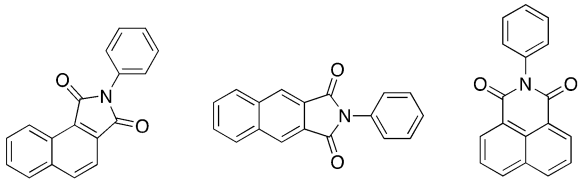

Figure 1. Chemical structures of isomeric *N*-phenyl-naphthalimides.

(2) the nature of substituents located on the naphthalene ring,[1,4−6,19,22,29,31] such as electron-withdrawing groups or electron-donating groups, and (3) the nature of substituents attached to the imide group. Regardless of the constitutional isomerism for *N*-aryl-1,2-NI, -2,3-NI, and -1,8-NI (Figure 1), a common similarity exists: electron-withdrawing groups (EWG) on either the naphthalene ring or phenyl ring promotes SW emission, and electron-donating groups (EDG) on both sides promote LW emission.[2,20,24] In addition, all NIs exhibit dual emission that is viscosity, temperature, and solvent dependent making them ideal probes for a number of analytical applications.[23,29]

Among *N*-aryl-NI isomers, the *N*-aryl-2,3-NIs have the highest potential for application in WOLEDs because of their high quantum yield, panchromatic emission, small molecular weight ideal for vacuum deposition, and easy synthesis and purification by recrystallization and sublimation.[2,6] Despite such promising applications of substituted *N*-aryl-2,3-NIs, relatively few fundamental studies regarding their photophysical and solvatochromic properties exist.[32] Herein, we present a comprehensive study into four promising dyes panchromatic fluorescent dyes. The four compounds investigated in this paper are listed in Chart 1, and denoted as F-OCH_3, F-2OCH_3, Cl-NH_2, and NO_2/Cl-NH_2, respectively. The synthesis of each one along with spectrometric characterization is described within the Supporting Information section of the manuscript. This investigation includes insights into their ground and excited states via density functional theory (DFT)/ time-dependent DFT (TD-DFT) calculations and experimental analyses that include solvent-dependent steady-state absorption and fluorescence data and excited state lifetimes. Finally, we describe a direct application of their photoluminescence toward WOLED fabrication and evaluation as potential electro-

Chart 1. Chemical Structures of *N*-Aryl-2,3-naphthalimides

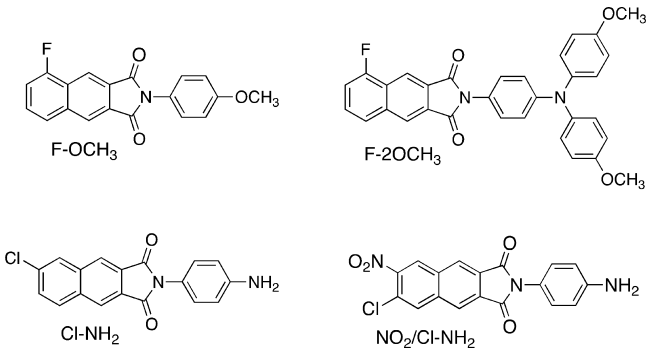

luminescent materials. The findings should provide insights toward further development of these small molecule systems with predictable outcomes in the transitional development from fundamental photoluminescence studies to electroluminescent materials.

EXPERIMENTAL SECTION

Materials. Hexane (HPLC grade), toluene (HPLC grade), ethyl acetate (HPLC grade), chloroform (HPLC grade), methylene chloride (HPLC grade), ethanol, acetonitrile (HPLC grade), dimethyl sulfoxide (DMSO, HPLC grade), methanol, and acetic acid were purchased from Fisher Scientific. All the other chemicals were purchased from Sigma-Aldrich.

General Characterizations. ^{1}H NMR spectra were obtained on a JEOL Eclipse+ 300 MHz and Bruker 400 MHz spectrometer. Chemical shifts (δ) are reported in parts per million (PPM) relative to TMS standard (0 ppm). Proton-decoupled ^{13}C NMR spectra were obtained on JEOL Eclipse 300+ (75 MHz) spectrometer. ^{13}C chemical shifts are reported relative to TMS. IR stretches are given in cm^{-1}; spectra were obtained on an Avatar 360 FTIR.

UV/Vis Steady-State Measurements. For fluorescence measurements, the concentration of each 2,3-NI solution was prepared so that the absorption at the wavelength of maximum absorption was in the range of 0.10−0.15. Fluorescence spectra were collected using SPEX Fluoromax-3, with xenon arc lamp in 10 mm quartz cells. UV/vis measurements were carried out on HP 8453 spectrometer with 10 mm quartz cuvette. Thin-layer chromatography (TLC) analysis was performed using Whatman adsorption silica gel plates (60 Å, F254, 2.50 MM).

Fluorescence Lifetime Measurements. Fluorescence emission spectra were taken with two instruments. The first set was taken with a PTI spectrofluorometer (Photon Technology International, NJ) with excitation and emission slits set for a 5 nm bandwidth at certain wavelength. The lifetime measurement is using an associated LED (310 nm) light source, the result is fitted according to the Instrument Response Function (IRF) through 1-to-4 exponent lifetime program by PTI Felix 32 software. The second set was acquired by using a Jobin Yvon FluoroLog spectrofluorometer (Horiba) equipped with a 450 W xenon lamp (250−700 nm) coupled to a monochromator, to provide a range of selected excitation wavelengths. The emission spectra were collected in a right-angle geometry and subsequently scaled for the excitation intensity, and corrected for spectral sensitivity of the detector. The PL QY has been determined using an integrating sphere with a 150 W xenon lamp coupled to a spectrometer (Solar,

DOI: 10.1021/acs.jpca.7b08110
J. Phys. Chem. A 2017, 121, 9708−9719

MSA-130) as an excitation source. The emission and excitation light is scattered diffusively in the integrating sphere and detected by using a CCD (Hamamatsu S10141-1108S) coupled to a second spectrometer (Solar, M266).

Fluorescence Quantum Yield. The room temperature luminescence quantum yields were measured at a single excitation wavelength referenced to quinine sulfate in sulfuric acid aqueous solution ($\Phi = 0.546$), and calculated according to the following equation.[33]

$$\Phi_{unk} = \Phi_{std}\left(\frac{I_{unk}}{I_{std}}\right)\left(\frac{A_{unk}}{A_{std}}\right)\left(\frac{n_{unk}}{n_{std}}\right)^2$$

where Φ_{unk} is the radiative quantum yield of the sample; Φ_{std} is the radiative quantum yield of the standard; I_{unk} and I_{std} are the integrated emission intensities of the sample and standard, respectively; A_{unk} and A_{std} are the absorption of the sample and standard at the excitation wavelength, respectively; and n_{unk} and n_{std} are the indexes of the refraction of the sample and standard solutions (pure solvents were assumed), respectively.

Cyclic Voltammetry. CV measurements in this study were conducted on a computer-controlled CH electrochemical analyzer with a conventional three-electrode cell setup under argon atmosphere in a deoxygenated anhydrous acetonitrile solution of 0.1 M tetrabutylammonium hexafluorophosphate (Bu_4NPF_6). A coiled Pt wire was used as the counter electrode, a 3 mm diameter glassy carbon as the working electrode, and an Ag/Ag^+ (0.01 M $AgNO_3$ in acetonitrile) pseudoreference electrode was used as the reference electrode. All the CVs were performed at room temperature. The sample with concentration of 10^{-4} M was dissolved in the solution. The CV curves were calibrated using the ferrocene/ferrocenium (Fc/Fc^+) redox couple as an internal standard, which was measured under the same condition after the measurement of samples. The CV measurements were achieved at a scan rate of 100 mV s^{-1}. The potentials in these CVs are plotted versus the ferrocenium/ferrocene redox couple. Each CV was recorded using an initial potential of −0.6 V, scanning cathodically to a switching potential of −2.6 V and then scanning anodically to a switching potential of +0.6 V with a final potential of −0.6 V.

OLEDs Fabrication and Characterization. The organic layers were sequentially deposited by thermal evaporation in a vacuum chamber. The background pressure of the evaporation was less than 2×10^{-6} mbar. The deposition rate of organic materials was kept 0.5−2.5 Å/s. Metals (magnesium, aluminum, or silver) were deposited onto the organic layer by thermal deposition, too. The rate of metal deposition was maintained at 2−5 Å/s. The layer thickness was monitored in situ using a quartz crystal oscillator in the chamber. The active area of the device was 9 mm^2 as defined by the homemade shadow mask. After the devices were fabricated, the EL spectrum was measured with an Avantes Spectrometer 2048L. The current−voltage characteristics of the devices were measured with Keithley 2400. The current density−voltage characteristics, and the electroluminescent spectra were measured at room temperature and under an ambient atmosphere.

RESULTS AND DISCUSSION

UV/Vis Absorption Measurements. The UV−vis absorption spectra of the four *N*-aryl-2,3-naphthalimides (Chart 1) included in this study are shown in Figure 2. To ensure the various absorption peaks were not due to aggregation, a series of spectra were taken on new dye F-2OCH_3 over a concentration range of 1×10^{-5} M to 1×10^{-4} M (see Supporting Information) and found to have the identical line shape even well above optical densities of one. Dye F-2OCH_3 shows a strong and structured absorption band around 340−360 nm, and a moderate and broad peak centered at 390 nm. The medium-intense absorption maxima for F-OCH_3 appear around 340 to 360 nm and in the case of Cl-NH_2 spectrum, a medium-intense peak around 360 nm is pronounced by a very broad absorbance. When dissolved in water, NO_2/Cl-NH_2 displays the largest degree of panchromatic absorption spectrum with three broad absorbance peaks centered around 370, 460, and 510 nm, respectively; the intensity of 370 nm is slightly stronger. All of the NI derivatives show broad absorption bands consistent with the presence of CT excited states.[4]

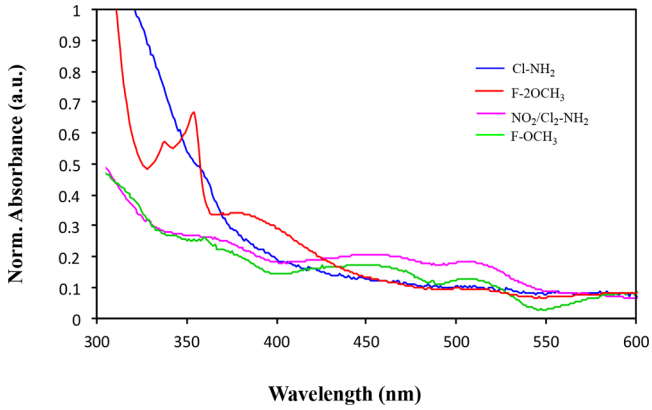

Figure 2. Normalized absorbance spectra of Cl-NH_2 and NO_2/Cl-NH_2 in water and F-OCH_3 and F-2OCH_3 in hexane.

To further investigate the nature of the excited states of the four NI derivatives, the effects of solvent polarity on the absorbance maxima were studied. The correlation between the solvent polarity and the absorption maximum shift is described by the Lippert equations eq 1 and 2.[34,4]

$$h\nu_{Abs} = h\nu_0^{Abs} - \frac{2\mu_g(\mu_e - \mu_g)}{a_0^3} \times f(\varepsilon, n) \quad (1)$$

In these equations, $h\nu_{Abs}$ and $h\nu_0^{Abs}$ are the corresponding energies in a given solvent and in the vacuum; μ_g and μ_e are dipole moments for a molecule in the ground and excited states, respectively; a_0 is the molecular Onsager radius; $f(\varepsilon,n)$ is a function that depends on the relative permittivity (ε) and refractive index (n) of the solvent and is described by equation eq 2. The energy difference between the ground and excited states is determined by the two terms: the first term is the low frequency polarizability of the solvent and the second term is the high frequency polarization of the solvent.

$$\Delta f(\varepsilon, n) = \frac{\varepsilon - 1}{2\varepsilon + 1} - \frac{n^2 - 1}{2n^2 + 1} \quad (2)$$

Application of the Lippert equations via plots of either the absorption or emission maxima versus the orientation polarization (Δf) of the solvent media gives an approximation of the fluorophore's sensitivity to solvent polarity. The slope of these plots could be positive, negative or zero. If the slope is positive, the excited state dipole moment is smaller than the dipole moment of the ground state ($\mu_e < \mu_g$), this situation occurs in compounds that exhibit n,π^* excited states. The absorption and

DOI: 10.1021/acs.jpca.7b08110
J. Phys. Chem. A 2017, 121, 9708−9719

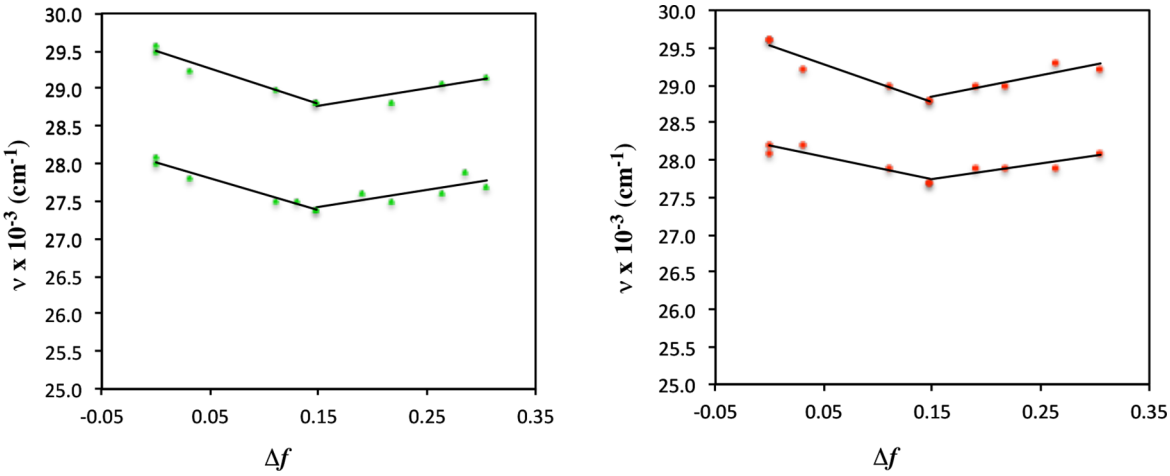

Figure 3. Lippert–Mataga plots of the absorbance of F-OCH_3 (left) and F-2OCH_3 (right) at both SW (top line, both plots) and LW (bottom line, both plots).

emission maxima are expected to blue-shift with increasing solvent polarity. If the slope is negative, the excited state dipole moment is larger than the dipole moment of the ground states ($\mu_e > \mu_g$), this situation occurs in molecules with charge transfer (CT) and π,π^* excited states. The absorption and emission maxima should display a red-shift as a result increasing solvent polarity. Finally, if the slope is zero, there is no net change in dipole moment ($\mu_e < \mu_g$) in both ground and excited states.

Figure 3 plots the changes in the absorption maxima ν_{max} of F-OCH_3 and F-2OCH_3 as a function of the solvent's f function. Cl-NH_2 and NO_2/Cl-NH_2 were not investigated using the Lippert–Mataga analysis because of their poor solubility in aprotic solvents.[34] The wavelength range of 340–360 nm was selected since these values represent the lowest energy absorption band with the expectation that such electronic transitions originate from frontier orbitals. Both 340 and 360 nm are denoted as short wave (SW) and long wave (LW) wavelength, respectively. Lippert–Mataga plots on F-OCH_3 and F-2OCH_3 showed similar results where both SW and LW absorption maxima displayed an initial red-shift (negative slope) with increasing solvent polarity. This trend occurs in compounds that exhibit CT and π–π^* excited states. However, upon increasing the polarity of the solvents, both SW and LW exhibit a blue-shift (positive slope); an observation consistent with n–π^* excited states. If the absorbed light produced only (n–π^*), a blue-shift in the absorption trend is expected. On the other hand, a trend toward red-shift in absorption is expected if the absorbed light generates (ICT and π–π^*). However, as determined by the Lippert analysis, the observation of both bathochromic and hypsochromic shifts of the absorbance maxima indicates mixed excited states. These results corroborate the conclusions of previous publications wherein the absorption of light produces primarily two excited states (n–π^* and π–π^*), and show different excited state characteristics based on the environmental polarity. The SW and LW of the absorbance maxima for both F-OCH_3 and F-2OCH_3 in solvents of various polarities are listed in the Supporting Information.

Fluorescence Measurements. The fluorescence spectra of all the *N*-aryl-2,3-naphthalimides (F-OCH_3, F-2OCH_3, Cl-NH_2, and NO_2/Cl-NH_2) are shown in Figure 4. All these solutions exhibited broad emission spectra over the range 400–700 nm upon corresponding excitation wavelengths. NI derivative F-OCH_3 in ethyl acetate was excited at 310 nm, and displays dual-

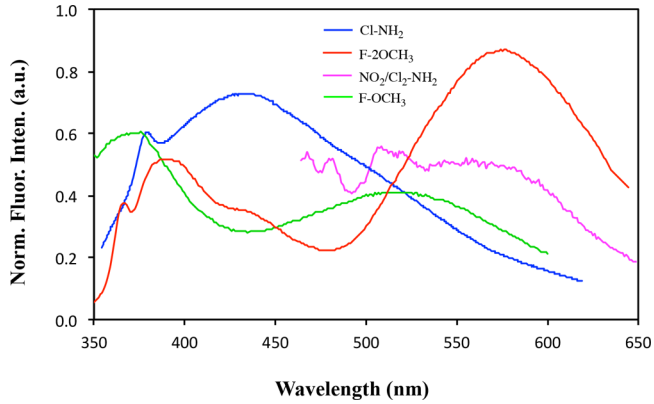

Figure 4. Fluorescence spectra of F-OCH_3 in EtOAc at λ_{ex} 310 nm, F-2OCH_3 in cyclohexane at λ_{ex} 330 nm; Cl-NH_2 in methanol at λ_{ex} 340 nm, and NO_2/Cl-NH_2 in water at λ_{ex} 430 nm. Hence, the emission data for NO_2/Cl-NH_2 appears truncated and begins 30 nm after 430 nm excitation wavelength.

fluorescence at SW (370 nm) and LW (520 nm). F-2OCH_3 in cyclohexane was excited at 330 nm with dual-fluorescence SW emission at 390 nm and LW emission at 570 nm. Comparing fluorescence spectra of F-OCH_3 and F-2OCH_3, both SW and LW emission bands of F-2OCH_3 are red-shifted because of the stronger electron-donating group on the *N*-aryl ring and extended conjugation. In less-polar aprotic solvents, both F-OCH_3 and F-2OCH_3 display dual-fluorescence. The LW emission was reduced significantly in polar (protic and aprotic) solvents for F-OCH_3 and F-2OCH_3, especially for F-2OCH_3, LW emission was completely quenched in polar solvents such as acetonitrile and dimethyl sulfoxide. Compared with the spectroscopic properties of F-OCH_3 and F-2OCH_3, NO_2/Cl-NH_2, and Cl-NH_2 displayed very different spectral features. In protic solvents such as water and methanol, NO_2/Cl-NH_2 exhibited panchromatic emission from 470 to 650 nm with an excitation wavelength of 430 nm, whereas Cl-NH_2 displayed a broader emission profile in similar solvent conditions. All fluorescence measurements were conducted at a concentration of 10^{-5} M. The quantum yields of F-OCH_3, F-2OCH_3, Cl-NH_2, and NO_2/Cl-NH_2 are 16%, 21%, 5%, and 46%, respectively.

To further investigate the nature of the excited states of these compounds, the effects of the solvent polarity on the emission

DOI: 10.1021/acs.jpca.7b08110
J. Phys. Chem. A 2017, 121, 9708–9719

maxima were also studied. The correlation between the solvent polarity and the emission maximum shift are described similarly to the absorption analysis by Lippert equations [4a],:[34,35]

$$h\nu_{Em} = h\nu_0^{Em} - \frac{2\mu_g(\mu_e - \mu_g)}{a_0^3} \times f(\varepsilon, n) \quad (3)$$

In these equations, $h\nu_{Em}$ and $h\nu_0^{Em}$ are the corresponding energies in a given solvent and in the vacuum; terms like μ_g, μ_e, a_0, and $f(\varepsilon,n)$ are detailed in the previous section. In contrast with the absorbance, the emitting fluorophore is exposed to the relaxed environment, which contains solvent molecules oriented around the dipole moment of the excited state. The high sensitivity to solvents is due to a charge shift. If the solvent is polar, then a species with charge separation (Intramolecular Charge Transfer, ICT) state may become the lowest energy state. In a nonpolar solvent the species without charge separation, the so-called locally excited state, may have the lowest energy. Hence, the role of solvent polarity is not only to lower the energy of excited states due to general solvent effects, but also to govern which state has the lowest energy. Figure 5

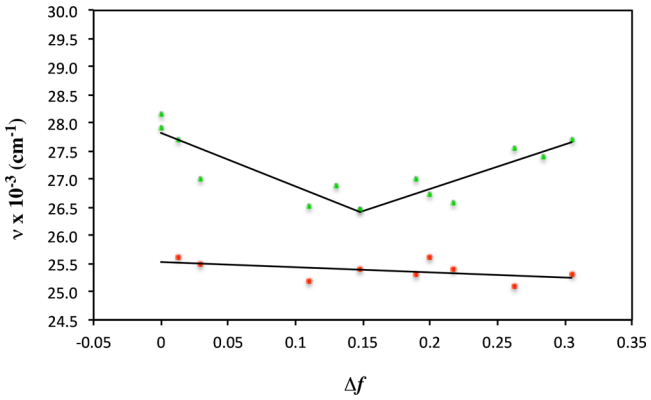

Figure 5. Lippert–Mataga plots of the SW fluorescence of F-OCH_3 (top) and F-2OCH_3 (bottom).

plots the changes in the SW fluorescence maxima ν_{max} of F-OCH_3 and F-2OCH_3 as a function of the solvent's f function. The fluorescence spectra in various solvents for these dyes are included in Figures S8 and S10 in the supporting info.

Figure 5 shows the Lippert–Mataga plot of SW of F-OCH_3 in various solvents giving a negative slope in less-polar solvents, and a positive slope in polar solvent. These results indicate that there are at least two different excited state species (π,π^* and n,π^*) responsible for the SW fluorescence. These results agree well with the characterization of the excited states acquired via optical absorption. However, the effect of solvent polarity on the emission is not always comparable to observations from absorption maxima. For example, F-2OCH_3 exhibits a bathochromic shift (4 nm) in nonpolar solvents and a hypsochromic shift (6 nm) in polar solvents for the absorption maximum, whereas a red shift of 40 nm is observed for its emission maximum at SW. Such trends point to an emissive state from F-2OCH_3 that differs from one produced upon light absorption. Thus, upon light absorption, it appears that both $n-\pi^*$ and $\pi-\pi^*$ are produced. With respect to SW emission, we therefore conclude that $\pi-\pi^*$ and charge transfer features predominate. In the computational section (*vide infra*), these assignments along with their excited state designations (S_1, S_2) are supported with the use of DFT and TD-DFT calculations.

Fluorescence at Long Wavelength (LW). The Lippert–Mataga graph shown in Figure 6 plots the LW emission maxima

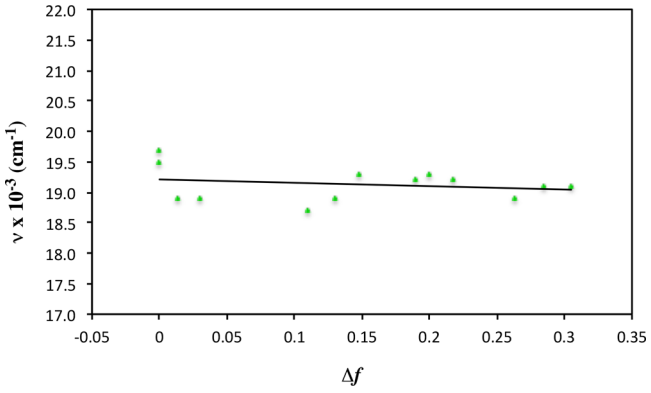

Figure 6. Lippert–Mataga plot of the LW fluorescence of F-OCH_3.

for F-OCH_3 in various solvents rather flat to slightly negative slope and is therefore not a strong indication of a polar CT possibly with $\pi-\pi^*$ character. For F-OCH_3, the observed solvatochromic behavior of LW fluorescence was consistent with Berces' results on the parent *N*-phenyl-2,3-naphthalimide.[23] For F-2OCH_3, LW emission was present only in hexane and toluene (Supporting Information). In more polar solvents, the LW emission was completely absent; whereas in comparisons with solvents hexane and toluene the LW fluorescence of F-2OCH_3 trended with an approximately 100 nm shift toward the red, providing a better possibility of an excited state of CT and π, π^* character. Within the limited range of solubility for F-2OCH_3, we compare LW emission maxima between F-2OCH_3 and F-OCH_3 to find that F-OCH_3 fluorescent peak occurs at 530 nm, whereas LW maxima for F-2OCH_3 occurs at 610 nm, we attribute the 80 nm bathochromic difference between these dyes to an increasing CT character from the stronger electron-donating moiety of the F-2OCH_3.[29]

Although the TICT mechanism has been attributed to several dual fluorescent dyes, our results support prior studies that point to an excited state with extended conjugation (ESEC). For a TICT mechanism to be considered, the emission from such a polar state occurs at long wavelengths and is strongly dependent on the solvent polarity.[35] In our case, the LW emission from F-OCH_3 shows a small variation in $\Delta\mu$ (4.1 D) between the ground state and the excited state, as deduced from the plot of ν_{max} versus $\Delta\phi$, and is therefore incompatible with an emission originating from a TICT-type species. Moreover, a rather large change in dipole moment for the molecule is expected via TICT when electric charge has been transferred from the donor moiety to the acceptor part of the molecule.[36] Such a change in dipole moment would cause a large shift (3000–5000 cm^{-1}) in the position of the fluorescence maximum.[23] However, only a 780 cm^{-1} shift was observed for F-OCH_3 when hexane was replaced by acetonitrile, thus lending support to the aforementioned ESEC excited state model.

Lifetime Measurements of the Fluorescence. To ascertain the number of potential excited states, fluorescent lifetime measurements were conducted in both polar and nonpolar solvents. For F-OCH_3, two excited states were identified for SW emission and one excited state attributed to LW emission (Figure 7). As tabulated below (Table 1) the two

DOI: 10.1021/acs.jpca.7b08110
J. Phys. Chem. A 2017, 121, 9708–9719

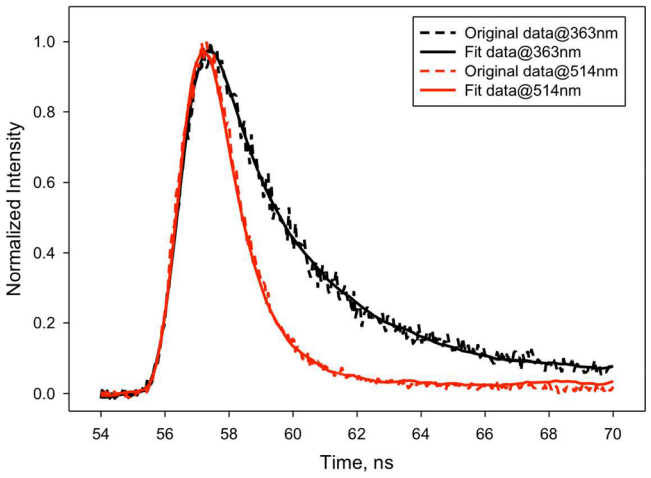

Figure 7. Fluorescence lifetime measurement of F-OCH_3 in hexane.

excited states responsible for SW emission are composed of 50% of 0.85 ns along with 50% of 3.2 ns in hexane. The parity of these excited states is altered in the case of acetonitrile at 60% of 0.29 ns and 40% of 2.3 ns and even greater disparity with CH_2Cl_2 at 10% of 0.44 ns and 90% of 2.9 ns. While these trends in SW excited state composition do not trend directly with solvent dielectric constant, solvent viscosity may play a role since hexane has the lowest viscosity (0.30 mPa·s) and dichloromethane is the most viscous (0.41 mPa·s) of the three solvents. Overall, these results comparing SW vs LW emission agree well with the predictions from the Lippert−Mataga analysis on both absorbance and emission maxima. Along with Lippert−Mataga analysis, we are able to assign the short-lived lifetime excited state (0.85, 0.44, and 0.29 ns) to (n−π*), and the relatively long-lived lifetime excited state (3.2, 2.9, and 2.3 ns) to (π−π*). Furthermore, these designations correlate with the assignments of Glusac et al. on related 4-substituted-1,8-naphthalimides.[4]

Whereas Lippert−Mataga analysis predicted at least one dominant character (π−π*) for the SW emission region of F-2OCH_3, the lifetime measurements within the SW emission region indicate that there are two excited states. However, for all these excited states in various solvents, there is predominantly one species. In ethyl acetate, the excited states of SW were composed of singlet-excited states of 3.4 ns (81%) and 33 ns (16.5%), and an additional yet negligible triplet state T_1 of 2.5%. In hexane and toluene, the dominant excited species are singlets 2.2 ns with concentration of 88.6%, and 2.3 ns with 72.8%, respectively. According to the predictions of Lippert−Mataga analysis, the character of this excited state consists of CT and π−π*. It is difficult to assign the character of the relatively long-lived excited states at this point. However, considering the species produced upon light absorption, this longer-lived excited state appears to exhibit n−π* character. Interestingly, a comparison between the above n−π* state lifetimes of F-OCH_3 and F-2OCH_3 indicates notably longer lifetimes for F-2OCH_3. While we cannot state with certainty, one factor that may account for these differences appears in the computational geometries of ground state versus excited state in the next section. Since F-2OCH_3 has a smaller angular change from 42° to 20° versus F-OCH_3 with an angular dynamic change of 42° to 16°, this finding suggests decreased internal conversion for F-2OCH_3 presumably due to a bulkier *N*-aryl group and corresponding reduced rotational freedom within the excited time frame.

Similar fluorescent lifetime trends were observed for Cl-NH_2 and Cl/NO_2−NH_2 where both SW and LW emissive components contribute to the broad-spectrum fluorescence. However, both of these dyes displayed a longer LW excited state lifetimes of 7.3 ns (10%) and 13.8 ns (78%) compared to SW at 1.2 ns (44%) and 2.84 ns (46%) for Cl-NH_2. The LW emission of Cl/NO_2−NH_2 recorded at 4.2 ns (59%), 9.7 (18%) relative to SW emission at 1.02 ns (19%) and 0.49 ns (7%). These longer excited state lifetimes correspond to brighter LW emission components for both systems thus leading to greater parity between LW and SW regions of the optical spectrum than either FOCH_3 or F-2OCH_3.

Time-Dependent (TD)-DFT Calculations. All of the calculations were performed with the Gaussian 09 software package.[37] The ground-states geometries were optimized using Becke's three-parameter hybrid exchange functional with the Lee−Yang−Parr correction functional (B3LYP) method[38] in conjunction with the 6-31G(d) basis set.[39] To validate the computational method, we compared the calculated electronic absorption maxima of these dyes with those obtained experimentally (Table 2). Absorption maxima were obtained by employing TD-DFT/6-31G(d) calculations. The singlet-excited geometry was calculated using TD-DFT.[40] The effects of solvation on the vertical excitation energies were computed with Tomasi's polarizable continuum model (PCM)[4,41−46] at the TD-B3LYP/6-31G(d) level of theory as implemented in Gaussian 09.

The calculated small oscillator strengths (f) for S_1 (transition between HOMO and LUMO) on F-OCH_3, F-2OCH_3, and Cl-NH_2 lend strong support for the formation of S_2 upon light

Table 1. Excited State Lifetime of F-OCH_3, F-2OCH_3 ClNH_2 and NO_2/Cl-NH_2 in Various Solvents along with Relative Concentrations, with Values Extracted from the Supporting Information

	τ_f (ns (%))	
dye	SW*	LW*
F-OCH_3	0.85 (50%); 3.2 (50%)[a]a	0.85 (100%)
	0.44 (10%); 2.9 (90%)[b]	0.42 (100%)
	0.29 (60%); 2.3 (40%)[c]	0.89 (100%)
F-2OCH_3	2.2 (88.6%); 18 (11.4%)[a]	0.08 (94.3%); 4.33 (5.7%)
	2.3 (72.8%); 9.8 (23.2%)[d]	–
	3.4 (81%); 33 (16.5%); T_1 (2.5%)[e]	–
Cl-NH_2	1.2 (44%); 2.84 (46%)[a]	7.3 (10%); 13.8 (78%)
NO_2/Cl-NH_2	0.49 (14%); 1.02 (38%)	4.2 (59%); 9.7(18%)[f]

[a]In hexane. [b]In CH_2Cl_2. [c]In acetonitrile. [d]In toluene. [e]In EtOAc. [f]DMSO.

DOI: 10.1021/acs.jpca.7b08110
J. Phys. Chem. A 2017, 121, 9708−9719

Table 2. Comparison of Experimental Absorption Maxima of 2,3-NIs with the Calculated S_1, S_2, and S_3 Excited States Using TD-DFT

		S_1		S_2		S_3	
compd	λ_{exp} (nm)	λ (nm)	ϕ_1	λ (nm)	f_2	λ (nm)	f_3
F-OCH_3	–	405[a]	0.0040	365	0.1358	326	0.2500
	355; 338	403[b]	0.0051	359	0.1364	333	0.4024
	363; 346.5	397[c]	0.0049	351	0.0049	336	0.5936
	360; 343	395[d]	0.0046	350	0.0040	334	0.5880
F-2OCH_3	–	581[a]	0.0014	518	0.1652	340	0.0061
	353; 337	577[b]	0.0016	507	0.2002	340	0.0350
	358; 345	564[c]	0.0015	486	0.2131	342	0.3187
	358; 341	559[d]	0.0014	479	0.2120	343	0.3144
ClNH_2	–	450[a]	0.0028	410	0.1697	323	0.1161
	–	461[c]	0.0036	401	0.2206	333	0.2636
	–	461[d]	0.0034	398	0.2116	334	0.2654
	365	448[e]	0.0033	393	0.2077	332	0.2492
NO_2/Cl-NH_2	–	671[a]	0.0915	452	0.1091	427	0.1240
	–	843[c]	0.1205	487	0.1475	465	0.1719
	–	864[d]	0.1161	489	0.1387	470	0.1691
	510; 480; 365	541[f]	0.0402	448	0.1042	377	0.2227

[a]Gas phase. [b]Heptane. [c]CH_2Cl_2. [d]Acetonitrile. [e]Methanol. [f]H_2O.

absorption. For F-OCH_3 and F-2OCH_3, the oscillator strengths point to S_2 and S_3. Upon light excitation, there are two different singlet-excited states formed. These findings agree well with Lippert−Mataga analysis on the absorbance maxima. Although the Lippert−Mataga analysis was not extended to NO_2/Cl-NH_2 due to solubility limitations, the absorbance predicted by TD-DFT/PCM for this dye is also consistent with the experimental findings. The experimental absorption maxima in water occur at 510, 480, and 365 nm; and the calculated absorbance peaks align at 541, 448, and 337 nm, respectively. The calculated oscillator strengths (f) for S_1, S_2, and S_3 in water also match well with the absorption intensity observed in water. For Cl-NH_2, it seems that the observed absorbance at 365 nm points to an S_2 excited state, although we cannot discount the possibility that an S_3 excited state was produced in the Franck−Condon state. The calculations also showed that S_1 and S_2 are mixed states for NO_2/Cl-NH_2, as are S_2 and S_3 for F-OCH_3.

Ground-State Optimizations and Absorbance Calculations. An X-ray analysis on the *N*-phenyl-2,3-naphthalimide reported the dihedral angle between the plane of the aryl and the naphthalene ring was 60°.[22] Figure 8 shows the ground states of the four 2,3-NIs and indicates a similar nonplanar dihedral angle of ∼45° between the naphthalene plane and the aryl rings. From the ground state optimization, the lengths of the two N−C bonds between the nitrogen atom and the carbon atoms of the two carbonyl groups are almost identical (1.42 Å) but shorter than N−C bond (1.43 Å) connecting *N*-phenyl.

However, for the excited states, the lengths of the two N−C bonds between the nitrogen atom and the carbon atoms of the two carbonyl groups increased to 1.49 Å. The N−C bond connecting *N*-phenyl decreased from 1.43 to 1.37 Å, which indicated higher bonder order (i.e., double-bond character) of these single bonds, and stronger conjugation between the two planes. These dihedral angles also decreased to 10, 20, 16, and 27°, respectively. Thus, the geometries of these excited states assume a more planar configuration, which supports the *excited state with the extended conjugation* (ESEC) model.

The calculated electron density distributions of the frontier orbitals are shown in Figure 9. The HOMOs for all four 2,3-NIs exhibit nonbonding characteristics because of the localized

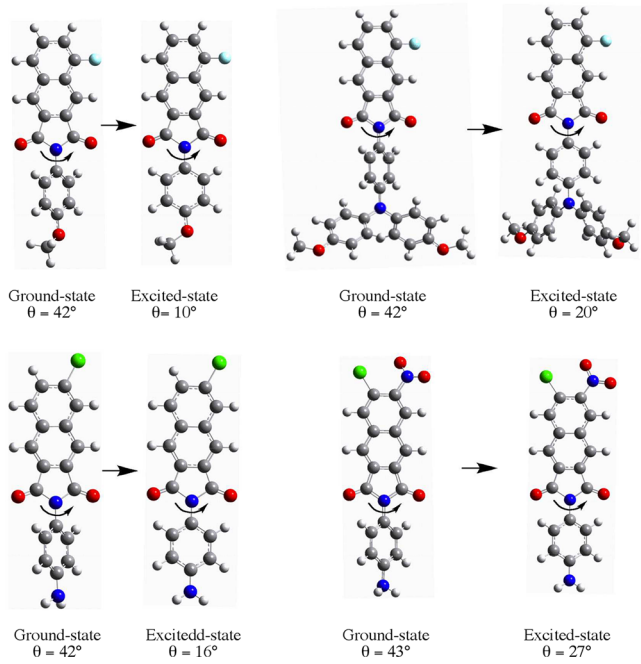

Figure 8. Calculated geometries for the ground- and excited states of 2,3-NIs. The angle θ represents the dihedral angle between the naphthalene plane and the aryl ring.

electron density distribution on carbonyl and methoxy groups. The electron density distribution of HOMO−1 on F-OCH_3 and Cl-NH_2 localized on the 2,3-naphthalene ring displays π−bonding character and the electron density distribution of HOMO−1 on F-2OCH_3 and NO_2/Cl-NH_2 located on the *N*-aryl ring shows π-bonding character as well. Both LUMO and LUMO+1 representations of all four *N*-2,3-NIs display a similar π^* character with virtual molecular orbital distribution located mainly on the 2,3-naphthalene ring. The molecular orbitals for HOMO and HOMO−1 illustrate patterns of electron density localized on either the *N*-aryl or 2,3-NI ring. Therefore, with the analysis on the electron density distributions of these frontier orbitals, it is reasonable to assign the $\pi-\pi^*$ charge

DOI: 10.1021/acs.jpca.7b08110
J. Phys. Chem. A 2017, 121, 9708−9719

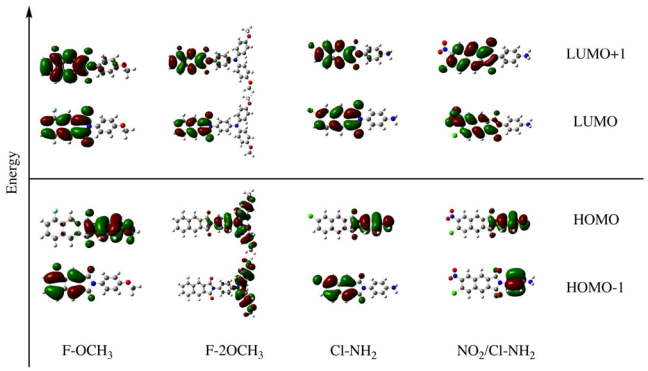

Figure 9. Calculated electron density distribution plots for the frontier orbitals of the four *N*-aryl-2,3-NIs.

transfer transition between HOMO and LUMO as S_1, and S_2 and n−π^* with the transition between HOMO and LUMO+1, respectively. S_3 exhibits π−π^* character with the transition occurring between HOMO−1 and LUMO on F-OCH_3 and Cl-NH_2, while the S_3 on F-2OCH_3 and NO_2/Cl-NH_2 exhibits charge transfer character. Combining the Lippert−Mataga analysis on the absorbance maxima, it seems reasonable to conclude that the excited states with mixed characters for the absorbance originate from S_3, and either S_1 or S_2.

Excited-State Optimizations and Fluorescence Calculations. To elucidate whether an S_1 or S_2 state was produced upon the absorption of light, the electronic absorption maxima of 2,3-NIs were calculated in various solvents and compared with those obtained experimentally. The computations were performed in both gas phase and with solvent effects, and were compared with the experimental results in various solvents (Table 3). We performed TD-DFT/PCM calculations on the emission maxima of these molecules in both gas-state and various solvents. The optimized geometries of the 2,3-NIs reveal a more planar structure. Since the report by Berces et al. on the parent *N*-phenyl-2,3-NI showed that only LW emission originates from the planar structure.[23] To elucidate the LW emission, we calculated fluorescence maxima of the *N*-aryl-2,3-NIs with the planar structure. The comparison of experimental fluorescence λ_{max} of the 2,3-NIs along with the calculated values using TD-DFT for S_1, S_2 and S_3 excited states are shown in Table 3. In comparing the Lippert−Mataga analysis on the LW emission maxima (Supporting Information) for both F-OCH_3 and limited values obtained for F-2OCH_3, we find that the slope is relatively flat and just slightly negative with indications of an excited state with weak ICT character. Interestingly, for both F-OCH_3 and F-2OCH_3 the calculated S_2 state with highest oscillator strength showed an opposite blue shift with increasing polarity of solvents. Thus, with relatively flat slope indications from our Lippert−Mataga analysis, computational results point to emission wavelengths correlating to oscillator strengths originative from an S_2 excited state. The calculated electron density distributions of the frontier orbitals of the different 2,3-NIs are presented in Figure 10. The calculated

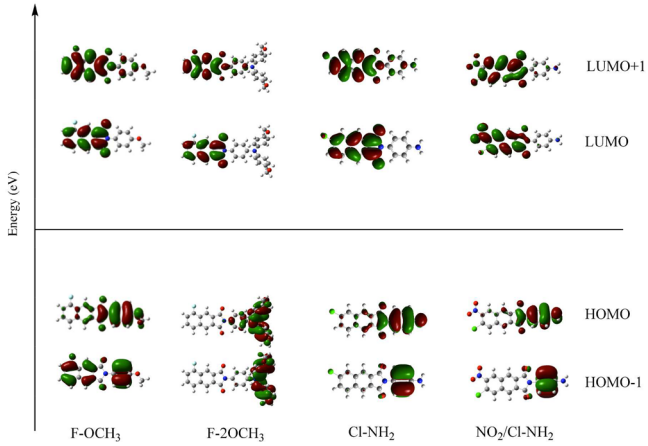

Figure 10. Calculated difference density plots for the frontier molecular orbitals of the excited 2,3-NIs. The red and green surfaces correspond to opposite amplitudes of the orbital wave function.

difference density plots represent excited states whereby occupied and virtual molecular orbitals have singly occupied

Table 3. Comparison of Experimental Fluorescence Maxima of the 2,3-NIs with the Calculated Wavelengths and Oscillator Strengths Using TD-DFT for S_1, S_2, and S_3 Excited States

		S_1		S_2		S_3	
compd	λ_{exp} (nm)	λ (nm)	ϕ_1	λ (nm)	f_2	λ (nm)	f_3
F-OCH_3	*a*	695	0.0039	466	0.3177	374	0.0006
	506; 355[b]	673	0.0052	457	0.3916	365	0.3449
	521; 376[c]	635	0.0048	431	0.3239	372	0.6272
	524; 361[d]	625	0.0044	424	0.2730	373	0.6623
F-2OCH_3	*a*	1151	0.0012	742	0.0973	486	0.0002
	390; 576[b]	1034	0.0012	681	0.1149	463	0.0002
	393[c]	903	0.0010	608	0.1200	434	0.0002
	395[d]	871	0.0009	590	0.1190	427	0.0002
ClNH_2	*a*	789	0.0030	519	0.3473	371	0.0003
	c	787	0.0039	502	0.4378	362	0.4318
	d	760	0.0036	491	0.4148	361	0.4217
	442, 525[c]	784	0.0036	495	0.4174	363	0.4378
NO_2/Cl-NH_2	*a*	852	0.0670	572	0.1712	452	0.0951
	c	877	0.0841	564	0.1681	455	0.1642
	d	870	0.0796	560	0.1533	452	0.1672
	492, 520, 595[f]	910	0.0792	574	0.1421	459	0.1943

[a]Gas phase. [b]Heptane. [c]CH_2Cl_2. [d]Acetonitrile. [e]Methanol. [f]H_2O.

DOI: 10.1021/acs.jpca.7b08110
J. Phys. Chem. A 2017, 121, 9708−9719

molecular orbitals (SOMOs). The S_2 state with charge-transfer in the polar solvent is stabilized to the extent that the energy level of S_2 becomes lowered significantly.[4] Assignment of the S_2 charge-transfer state to the HOMO to LUMO+1 transition is also consistent with Berces' results.[29] For NO_2/Cl-NH_2, the dihedral angle between the naphthalene ring and the aryl ring optimized to 27°. The small dihedral angle changes (15°) from that of the ground state (dihedral of 42°) was not significant to change the electron distribution dramatically on the frontier orbitals of the excites states. Therefore, the multiexcited states in the absorbance cause multiemission maxima. These results are supported by the large oscillator strengths (f) of S_1, S_2, and S_3 in both calculated absorbance and emission maxima, which agreed well with the experimental broad absorbance and emission spectra.

In comparing the Lippert−Mataga analysis of the emission maxima, the changes in the sign of the graphical slope indicate that the excited states emitting in the SW region have a mixed excited state character of n,π^* and π,π^*. Therefore, it is difficult to explain the mixed characters of the SW emission with only a planar structure. Compared with the Lippert−Mataga analysis on the excited states of both absorbance and emission maxima, the spectral features of both absorbance and emission maxima at SW revealed similar results. Therefore, it is reasonable to assume that the SW emission originates from a geometry that approximates the ground state, and differs from the planar excited state geometry.

Electroluminescent Device Fabrication and Measurements. With our two communications among the first reported *N*-aryl-2,3-napthalimides panchromatic fluorescent dyes, the considerable number of citations prompted us to expand these photoluminescent solvent studies to electroluminescent WOLEDs.[1,3] Since those early entries, relatively few small-molecule dyes have been reported to display white light emission.[47−55] The widely used approach for a single chromophore to achieve white electroluminescence is taken via short-wavelength fluorescence from the electron−hole recombination in an individual molecule and the broad longer-wavelength fluorescence from the intermolecular interactions. The intermolecular interactions usually originate from the formation of excimers, electromers, and aggregates.[56] However, these strategies suffer from some inherent problems. For example, the formation of some intermolecular species decreases the quantum yields of the WOLEDs. Details for the optimization and fabrication of an OLED device via a series of comparisons between solution and solid-state photoluminescent studies are described in the Supporting Information. This section includes determination of the band gaps for the four *N*-aryl-napthalimide dyes from cyclic voltammetry measurements along with their thin-film deposition via high-vacuum thermal deposition. Following several different fabrication designs and iterations of various layered systems, a four-layer structure (Figure 11) was fabricated for optimal performance (see Supporting Information for prior device layering and fabrication).

A Four-Layer Structure OLED. The optimized devices have a four layer structure of ITO/m-MTDATA [4,4′,4″ tris(*N*-3-methylphenyl-*N*-phenylamino)triphenylamine] (60 nm)/NPB (20 nm)/EM (100 nm)/Alq_3 (20 nm)/LiF (1 nm)/Al (300 nm). m-MTDATA is a well-accepted hole injection and transportation material.[57] The HOMO and LUMO energy levels of m-MTDATA are 5.1 and 1.9 eV, respectively. With HOMO energy level of 5.1 eV, lying between the HOMO of

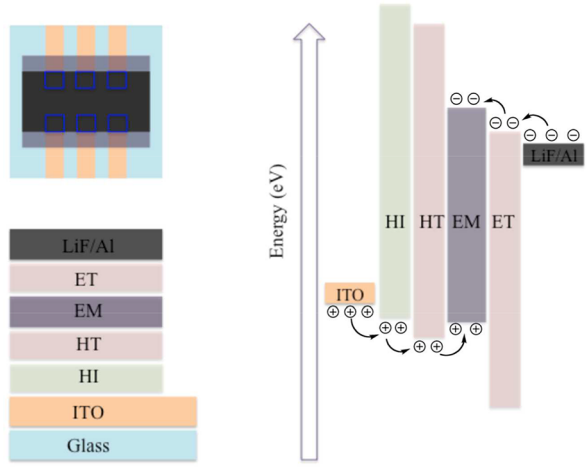

Figure 11. Four-layer structure WOLED along with energy levels combined with work functions of cathode and anode.

ITO (4.7 eV) and NPB (5.4 eV), the hole injection and transportation ability of these devices would be improved. With such a high LUMO energy level, m-MTDATA could also serve as the electron blocking layer for the devices. Device 1 was fabricated with emissive material F-OCH_3, device 2 with F-2OCH_3, device 3 from Cl-NH_2, and device 4 with NO_2/Cl-NH_2. The $J-V$ and electroluminescence spectra devices 1 and 2 are shown in Figure 12.

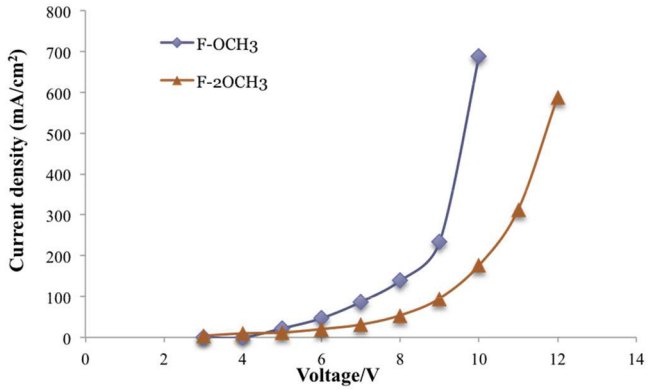

Figure 12. Current density−voltage characteristics for the device 1 and 2.

The estimated turn-on voltages for device 1 and 2 were lowered to 5 and 4 V, respectively, which indicated that the charge injection of the devices was improved by inserting the fourth layer as a hole-injection layer. The light emission from devices 1 and 2 showed the same color. Devices 3 and 4, (in Supporting Information) displayed no electroluminescent response. The possible formation of homogeneous films under thermal deposition conditions may be responsible, as the observed emission was too dim to measure.

The EL of device 2 is shown above (Figure 13), however, instead of white light emission, orange-EL was observed for this device. Compared with the solid-state photoluminescence from the previous studies, the SW peak at 400 nm disappeared in the EL spectrum. A likely reason that can account for this observation points to the SW emission of F-2OCH_3 which originates from a different but higher orbital energy level. The estimated energy gap difference between the SW and LW

DOI: 10.1021/acs.jpca.7b08110
J. Phys. Chem. A 2017, 121, 9708−9719

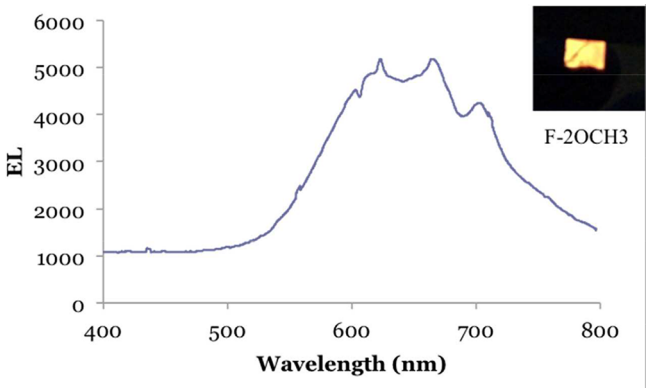

Figure 13. Electroluminescence spectrum for device 2 and a photo of the device in OLED operation

photoluminescence is about 1 eV. Therefore, with such a large energy barrier (1 eV) it becomes difficult to inject electrons and concomitant holes to this energy level. For device 1, a greenish white light emission was observed, however, with a resulting EL spectrum that was too low to record. From an atom economy analysis, it is noteworthy that the observed EL spectrum from the smaller heteroatomic architecture of F-2OCH$_3$ ($C_{32}H_{23}N_2O_4F$) is on par if not more broadly emissive than rubrene (5,6,11,12-tetraphenyltetracene), a red-colored $C_{42}H_{28}$ polycyclic aromatic hydrocarbon, which displays an orange-color EL.[56]

CONCLUSIONS

To summarize, a two-part investigation was reported into the excited-state properties of a series of *N*-aryl-2,3-NIs along with fabrication and electroluminescence measurements of these dyes. These *N*-aryl-2,3-NIs were chosen for their ability to display two or more emission bands of equal parity; otherwise known as panchromatic fluorescence. Upon gathering a series of steady-state absorption and fluorescence spectra from these 2,3-NI derivatives in solvents of prescribed polarities and complementary TD-DFT calculations, we found that the absorption of light generated the rather exceptional S_2 and S_3 excited states. Using the Lippert−Mataga analysis along with TD-DFT calculations, the excited states were determined to be n,π^* and π,π^*. This approach led to assigning the character of the excited states at SW emission for F-OCH$_3$ to be a mixture of n,π^* and π,π^*, and the character of the excited state at SW emission for F-2OCH$_3$ to be π,π^*. The character of LW emission for both F-OCH$_3$ and F-2OCH$_3$ was less certain as the Lippert−Mataga slopes were flat to slightly negative. While some scatter was observed from the trend line analyses, it should be noted that certain assumptions are made regarding Lippert−Mataga analyses. One assumption, that the dye under investigation is spherical in shape, may be relevant to these studies since *N*-aryl-2,3-naphthalimdes feature a longer or high aspect ratio relative to other fluorophores. The Lippert−Mataga analyses on Cl-NH$_2$ and NO$_2$/Cl-NH$_2$ was not available due to their poor solubility in nonaqueous solvents. Using fluorescence lifetime measurements, we concluded that a mixture of excited states comprises the SW emission of F-OCH$_3$ and F-2OCH$_3$, and one dominant charge transfer character state responsible for LW emission. These spectral characterizations are supported by the excellent agreement between the experimental absorption and emission maxima for all 2,3-NIs with those calculated using TD-DFT method. The TD-DFT calculations on the geometries of the excited states indicated that the excited state showed a planar structure. The origin of both the SW and LW emission were correlated to specific geometries such that the SW emission originates from an non-planar or twisted structure in the excited state, and LW emission originates from an excited state of coplanar structure. For F-OCH$_3$ and F-2OCH$_3$, which display dual fluorescence in nonpolar solvents, free-rotation of the bond between the imide-N−C-aryl ring was found to be critical toward producing dual fluorescence. For Cl-NH$_2$ and NO$_2$/Cl-NH$_2$, which display panchromatic emission in polar and protic solvents, solvent stabilization through H-bonding is necessary toward displaying panchromatic emission.

The quantum yields of these dyes in solid state decreased significantly compared with studies carried out in solution. Low quantum yield in the solid-state could be attributed to the poor performance of OLEDs electroluminescence. Because of their small architectures and low molecular weights, all of the dyes investigated in this study readily formed good films under ultrahigh vacuum deposition. The molecular energy levels of these compounds (HOMO and LUMO) were measured with cyclic voltammetry. Band gaps were also measured in both electrochemical and optical methods and results indicate that the HOMOs of these compounds matched well with the anode (ITO work function), and their LUMOs matched well with the cathode (LiF/Al). To fully study the electroluminescence of the four dyes, we designed and fabricated three devices; two of these are described within the Supporting Information. Of these devices, the four-layer structure device displayed the best performance in terms of parameters used to characterize EL. The electroluminescent spectra of these devices also indicated that the dual-fluorescence readily observed in solution, disappeared in the solid-state. A plausible explanation appears to stem from an inability to inject electrons to the higher LUMO+1 orbitals; a process observed in the solution phase. Hence, the short wavelength fluorescence peak, a key component to panchromatic luminescence, disappeared in the OLED device.

ASSOCIATED CONTENT

Supporting Information

The Supporting Information is available free of charge on the ACS Publications website at DOI: 10.1021/acs.jpca.7b08110.

Synthetic procedures for dual and panchromatic fluorescence dyes, spectrometric characterization such as ^{1}H and ^{13}C NMR, and HRMS for dyes **9**-**15**, plots for fluorescent lifetime decay and tables listing lifetime percentages and lifetimes, data tables for Lippert−Mataga graphical analysis, both fluorescence and absorbance plots of the dyes in solvents of varying polarity, and solid-state absorbance and photoluminescence spectra, cyclic voltammetry data, and methodology toward preparation of OLED devices (PDF)

AUTHOR INFORMATION

Corresponding Author

*(M.D.H.) E-mail: michael.heagy@nmt.edu.

ORCID

Michael D. Heagy: 0000-0002-4519-078X

Notes

The authors declare no competing financial interest.

DOI: 10.1021/acs.jpca.7b08110
J. Phys. Chem. A 2017, 121, 9708−9719

■ ACKNOWLEDGMENTS

Acknowledgment is made to the donors of the American Chemical Society Petroleum Research Fund, Grant 50709-ND4, for support of this research. NSF award #IIA-1301346 is acknowledged for support of fluorescence spectroscopy instrumentation. M.D.H. wishes to thank Dr. Gabriel A. Montaño, and Dr. Yongming Tian of the Center for Integrated Nanotechnologies, Los Alamos National Laboratory, Los Alamos NM. L.B. wishes to thank Dr. Sally Pias of the Department of Chemistry, New Mexico Tech, and also Mr. Ken Sherrel of the Department of Chemistry and Chemical Biology, University of New Mexico, for HRMS analysis. M.D.H. thanks Dr. Virginia Chang for her assistance in obtaining publication quality spectral and graphical figures.

■ REFERENCES

(1) Nandhikonda, P.; Begaye, M. P.; Cao, Z.; Heagy, M. D. Discovery of Dual Fluorescent 1,8-Naphthalimide Dyes Based on Balanced Seesaw Photophysical Model. *Chem. Commun.* **2009**, *33*, 4941−4943.

(2) Nandhikonda, P.; Begaye, M. P.; Cao, Z.; Heagy, M. D. Frontier Molecular Orbital Analysis of Dual Fluorescent Dyes: Predicting Two-Color Emission in *N*-Aryl-1,8-Naphthalimides. *Org. Biomol. Chem.* **2010**, *8*, 3195−3201.

(3) Nandhikonda, P.; Heagy, M. D. An Organic White Light-Emitting Dye: Very Small Molecular Architecture Displays Panchromatic Emission. *Chem. Commun.* **2010**, *46*, 8002−8004.

(4) Kucheryavy, P.; Li, G.; Vyas, S.; Hadad, C.; Glusac, K. D. Electronic Properties of 4-Substituted Naphthalimides. *J. Phys. Chem. A* **2009**, *113*, 6453−6461.

(5) Alexiou, M. S.; Tychopoulos, V.; Ghorbanian, S.; Tyman, J. H.; Brown, R. G.; Brittain, P. I. The UV-Visible Absorption and Fluorescence of Some Substituted 1,8-Naphthalimides and Naphthalic Anhydrides. *J. Chem. Soc., Perkin Trans. 2* **1990**, *2*, 837−842.

(6) Nandhikonda, P.; Heagy, M. D. Dual Fluorescent *N*-Aryl-2,3-naphthalimides: Applications in Ratiometric DNA Detection and White Organic Light-Emitting Devices. *Org. Lett.* **2010**, *12*, 4796−4799.

(7) Saito, I.; Takayama, M.; Kawanishi, S. Photoactivable DNA-Cleaving Amino Acids − Highly Sequence Selective DNA Photocleavage by Novel L-Lysine Derivatives. *J. Am. Chem. Soc.* **1995**, *117*, 5590−5591.

(8) Saito, I.; Takayama, M.; Sugiyama, H.; Nakatani, K.; Tsuchida, A.; Yamamoto, M. Photoinduced DNA Cleavage via Electron Transfer − Demonstration that Guanine Residues Located 5′ to Guanine are the Most Electron-Donating Sites. *J. Am. Chem. Soc.* **1995**, *117*, 6406−6407.

(9) Chanh, T. C.; Lewis, D. E.; Allan, J. S.; Sogandares-Bernal, F.; Judy, M. M.; Utecht, R. E.; Matthews, J. L. Neutralization of HIV-1 and Inhibition of HIV-1 Induced Cyncitia by 1,8-Naphthalimide Photoactive Compound. *AIDS Res. Hum. Retroviruses* **1993**, *9*, 891−896.

(10) Zhang, J.; Woods, R. J.; Brown, P. B.; Lee, K. D.; Kane, R. R. Synthesis and Photochemical Protein Crosslinking Studies of Hydrophilic Naphthalimides. *Bioorg. Med. Chem. Lett.* **2002**, *12*, 853−856.

(11) Skurla, C. P.; Perera, A.; Towe, C. T.; Robertson, P. R.; Healy, J. L.; Kane, R. R. Development of Photochemical Method for Meniscal Repair: A Preliminary Study. *J. Biomech.* **2007**, *40*, 220−224.

(12) Hasharoni, K.; Levanon, H.; Greenfield, S. R.; Gosztola, J.; Svec, W. A.; Wasielewski, M. R. Radical Pair and Triplet State Dynamics of a Photosynthetic Reaction-Center Model Embeded in Isotropic Media and Liquid Crystals. *J. Am. Chem. Soc.* **1996**, *118*, 10228−10235.

(13) Kolosov, D.; Adamovich, V.; Djurovich, P.; Thompson, M. E.; Adachi, C. 1,8-Naphthalimides in Phosphorescent Organic LEDs: The Interplay Between Dopant, Exciplex, and Host Emission. *J. Am. Chem. Soc.* **2002**, *124*, 9945−9954.

(14) Ramachandram, B.; Saroja, G.; Sankaran, B.; Samanta, A. Unusually High Fluorescence Enhancement of Some 1,8-Naphthalimide Derivatives Induced by Transition Metal Salts. *J. Phys. Chem. B* **2000**, *104*, 11824−11832.

(15) He, H.; Mortellaro, M. A.; Leiner, M. J. P.; Fraatz, R. J.; Tusa, J. K. A Fluorescent Sensor with High Selectivity and Sensitivity for Potassium in Water. *J. Am. Chem. Soc.* **2003**, *125*, 1468−1469.

(16) Guo, X.; Qian, X.; Jia, L. A Highly Selective and Sensitive Fluorescent Chemosensor for Hg2+ in Neutral Buffer Aqueous Solution. *J. Am. Chem. Soc.* **2004**, *126*, 2272−2273.

(17) Nandhikonda, P.; Heagy, M. D. An Abiotic Fluorescent Probe for Cardiac Troponin I. *J. Am. Chem. Soc.* **2011**, *133*, 14972−14974.

(18) Elbert, J. E.; Paulsen, S.; Robinson, L.; Elzey, S.; Klein, K. A Study of 4-(Alkylamino) Substitued 1,8-naphthalimide Fluoroionophores. *J. Photochem. Photobiol., A* **2005**, *169*, 9−19.

(19) Hui Bon Hoa, G.; Kossanyi, J.; Demeter, A.; Biczok, L.; Berces, T. Pressure Dependence of the Dual Luminescence of Twisting Molecules. The Case of Substituted 2,3-Naphthalimides. *Photochem. Photobiol. Sci.* **2004**, *3*, 473−482.

(20) Cao, H.; Chang, V.; Hernandez, R.; Heagy, M. D. Matrix Screening of Substituted *N*-Aryl-1,8-Naphthalimides Reveals New Dual Fluorescent Dyes and Unusually bright Pyridine Derivatives. *J. Org. Chem.* **2005**, *70*, 4929−4934.

(21) Inoue, Y.; Jiang, P.; Tsukada, E.; Wada, T.; Shimizu, H.; Tai, A.; Ishikawa, M. Unique Dual Fluorescence of Sterically Congested Hexaalkyl Benzenhexcarboxylates: Mechanism and Application to Viscosity Probing. *J. Am. Chem. Soc.* **2002**, *124*, 6942−6949.

(22) Dromzee, Y.; Kossanyi, J.; Wintgens, V.; Valat, P.; Biczok, L.; Demeter, A.; Berces, T. Crystal and Molecular Structure of N-Phenyl Substituted 1,2-, 2,3- and 1,8-Naphthalimides. *Z. Kristallogr. - Cryst. Mater.* **1995**, *210*, 760−765.

(23) Valat, P.; Wintgens, V.; Kossanyi, J.; Biczok, L.; Demeter, A.; Berces, T. Influence of Geometry on the Emitting Properties of 2,3-Naphthalimides. *J. Am. Chem. Soc.* **1992**, *114*, 946−953.

(24) Wintgens, V.; Valat, P.; Kossanyi, J.; Demeter, A.; Biczok, L.; Berces, T. Spectroscopic Properties of Aromatic Dicarboximides Part 3: Substituent Effect on the Photophysical Properties of *N*-Phenyl-2,3-Naphthalimides. *J. Photochem. Photobiol., A* **1996**, *93*, 109−117.

(25) Pardo, A.; Poyato, J. M. L.; Martin, E.; Camacho, J. J.; Reyman, D.; Brana, M. F.; Castellano, J. M. Solvent Effects on the Photophysical Properties of *N*-Substituted 1,8-Naphthalimide Derivatives. *J. Photochem. Photobiol., A* **1989**, *46*, 323−328.

(26) Pardo, A.; Martin, E.; Poyato, J. M. L.; Camacho, J. J.; Brana, M. F.; Castellano, J. M. Synthesis and Photophyeical Properties of Some *N*-Substituted-1,8-Naphthalimides. *J. Photochem. Photobiol., A* **1987**, *41*, 69−78.

(27) Pardo, A.; Poyato, J. M. L.; Martin, E. Photophysical Properties of 1,8-Naphthalimide Derivatives. *J. Photochem.* **1987**, *36*, 323−329.

(28) Middleton, R. W.; Parrick, J.; Clarke, E. D.; Wardman, P. Synthesis and Fluorescence of *N*-Substituted-1,8-Naphthalimides. *J. Heterocycl. Chem.* **1986**, *23*, 849−855.

(29) Demeter, A.; Berces, T.; Biczok, L.; Wintgens, V.; Valat, P.; Kossanyi, J. Comprehensive Model of the Photophysics of *N*-Phenylnaphthalimides: The Role of Solvent and Rotational Relaxation. *J. Phys. Chem.* **1996**, *100*, 2001−2011.

(30) Wintgens, V.; Valat, P.; Kossanyi, J.; Demeter, A.; Biczok, L.; Berces, T. Spectroscopic Properties of Aromatic Dicarboximides. Part 4. On the Modification of Fluorescence and Intersystem Crossing Processes of Molecules by Electron-Donating Methoxy Groups at Different Positions. The Case of 1,8-Naphthalimides. *New J. Chem.* **1996**, *20*, 1149−1158.

(31) Wintgens, V.; Valat, P.; Kossanyi, J.; Biczok, L.; Demeter, A.; Berces, T. Spectroscopic properties of aromatic dicarboximides. Part 1. -N-H and *N*-Methyl-Substituted Naphthalimides. *J. Chem. Soc., Faraday Trans.* **1994**, *90*, 411−421.

(32) Demeter, A.; Ravasz, L.; Berces, T. Influence of Hydrogen Bond Formation on the Photophysics of *N*-(2,6-Dimethylphenyl)-2,3-Naphthalimide. *J. Phys. Chem. A* **2004**, *108*, 4357−4364.

(33) Ye, K.; Wang, J.; Sun, H.; Liu, Y.; Mu, Z.; Li, F.; Jiang, S.; Zhang, J.; Zhang, H.; Wang, Y.; Che, C.-M. Supramolecular Structures and

DOI: 10.1021/acs.jpca.7b08110
J. Phys. Chem. A 2017, 121, 9708−9719

Assembly and Luminescent Properties of Quinacridone Derivatives. *J. Phys. Chem. B* **2005**, *109*, 8008−8016.
(34) Lippert−Mataga Analysis Studies on the General Effects of Solvents: Protic solvents with other interactions such as hydrogen bonding or formation of charge transfer states, are sometimes detected as deviations from the general theory. See: Lakowicz, J. R. *Principles of Fluorescence Spectroscopy*; Springer Science + Business Media: New York, NY, 2006.
(35) Rettig, W. Charge Separation in Excited States of Decoupled Systems-TICT Compounds and Implications Regarding the Development of New Laser Dyes and the Primary Process of Vision and Photosynthesis. *Angew. Chem., Int. Ed. Engl.* **1986**, *25*, 971−988.
(36) Rettig, W. Application of a Simplified Microstructural Solvent Interaction Model to the Solvatochromism of Twisted Intramolecular Charge Transfer (TICT) States. *J. Mol. Struct.* **1982**, *84*, 303−327.
(37) Frisch, M. J.; Trucks, G. W.; Schlegel, H. B.;et al. *Gaussian 09, Revision D.01*; Gaussian, Inc.: Wallingford CT, 2009.
(38) Becke, A. D. Density-Functional Thermochemistry. III. The Role of Exact Exchange. *J. Chem. Phys.* **1993**, *98*, 5648−5652.
(39) Francl, M. M.; et al. Self-Consistent Molecular Orbital Methods. XXIII. A Polarization-Type Basis Set for Second-Row Elements. *J. Chem. Phys.* **1982**, *77*, 3654−3665.
(40) Foresman, J. B.; Head-Gordon, M.; Pople, J. A.; Frisch, M. J. Toward a Systematic Molecular Orbital Theory for Excited States. *J. Phys. Chem.* **1992**, *96*, 135−149.
(41) Barone, V.; Cossi, M.; Tomasi, J. A New Definition of Cavities for the Computation of Solvation Free Energies by the Polarizable Continuum Model. *J. Chem. Phys.* **1997**, *107*, 3210−3221.
(42) Barone, V.; Cossi, M.; Tomasi, J. Geometry Optimization of Molecular Structures in Solution by the Polarizable Continuum Model. *J. Comput. Chem.* **1998**, *19*, 404−417.
(43) Cossi, M.; Barone, V. Analytical Second Derivatives of the Free Energy in Solution by Polarizable Continuum Models. *J. Chem. Phys.* **1998**, *109*, 6246−6254.
(44) Cossi, M.; Barone, V.; Cammi, R.; Tomasi, J. *Ab Initio* Study of Solvated Molecules: a New Implementation of the Polarizable Continuum Model. *Chem. Phys. Lett.* **1996**, *255*, 327−335.
(45) Cramer, C. J.; Truhlar, D. G. Implicit Solvation Models: Equilibria, Structure, Spectra, and Dynamics. *Chem. Rev.* **1999**, *99*, 2161−2200.
(46) Tomasi, J.; Persico, M. Molecular Interactions in Solution: An Overview of Methods Based on Continuous Distributions of the Solvent. *Chem. Rev.* **1994**, *94*, 2027−2094.
(47) Pati, A. K.; Gharpure, S. J.; Mishra, A. K. White Light Emission in Butadiyne Bridged Pyrene-Phenyl Hybrid Fluorophore: Understanding the Photophysical Importance of Diyne Spacer and Utilizing the Excited-State Photophysics for Vapor Detection. *J. Phys. Chem. A* **2016**, *120*, 5838−5847.
(48) Sakai, K.; Tsuchiya, S.; Kikuchi, T.; Akutagawa, T. An ESIPT Fluorophore with a Switchable Intramolecular Hydrogen Bond for Applications in Solid-State Fluorochromism and White Light Generation. *J. Mater. Chem. C* **2016**, *4*, 2011−2016.
(49) Angioni, E.; Chapran, M.; Ivaniuk, K.; Kostiv, N.; Cherpak, V.; Stakhira, P.; Lazauskas, A.; Tamulevicius, S.; Volyniuk, D.; Findlay, N. J.; Tuttle, T.; Grazulevicius, J. V.; Skabara, P. J. A Single Emitting Layer White OLED Based on Exciplex Interface Emission. *J. Mater. Chem. C* **2016**, *4*, 3851−3856.
(50) Sarkar, S. K.; Kumar, G. R.; Thilagar, P. White Light Emissive Molecular Siblings. Chem. *Chem. Commun.* **2016**, *52*, 4175−4178.
(51) Mukherjee, S.; Thilagar, P. Organic White-Light Emitting Materials. *Dyes Pigm.* **2014**, *110*, 2−27.
(52) Yang, Q.-Y.; Lehn, J.-M. Bright White-Light Emission from a Single Organic grCompound in the Solid State. *Angew. Chem., Int. Ed.* **2014**, *53*, 4572−4577.
(53) Fujii, M.; Namba, M.; Yamaji, M.; Okamoto, H. Solvent-Induced Multicolour Fluorescence of Amino-Substituted 2,3-Naphthalimides Studied by Fluorescence and Transient Absorption Measurements. *Photochem. Photobiol. Sci.* **2016**, *15*, 842−850.
(54) Brancato, G.; Signore, G.; Neyroz, P.; Polli, D.; Cerullo, G.; Abbandonato, G.; Nucara, L.; Barone, V.; Beltram, F.; Bizzarri, R. Dual Fluorescence through Kasha's Rule Breaking: An Unconventional Photomechanism for Intracellular Probe Design. *J. Phys. Chem. B* **2015**, *119*, 6144−6154.
(55) Ganin, E. V.; Masunov, A. E.; Siminel, A. V.; Fonari, M. S. Preparation, Characterization, and Electronic Structure of Asymmetric Isonaphthalimide: Mechanism of Dual Fluorescence in Solid State. *J. Phys. Chem. C* **2013**, *117*, 18154−18162.
(56) Bao, L.; Heagy, M. D. A Review of Single White-Light Emitters: The Quest for Picture Perfect Dyes in the Next Generation of Single Layer WOLED Displays. *Curr. Org. Chem.* **2014**, *18*, 740−772.
(57) Xie, W.; Wu, Z.; Hu, W.; Zhao, Y.; Li, C.; Liu, S. Low-Voltage Top-Emitting Organic Light-Emitting Devices with an Organic Double-Heterojunction Structure. *Semicond. Sci. Technol.* **2005**, *20*, 443−445.

DOI: 10.1021/acs.jpca.7b08110
J. Phys. Chem. A 2017, 121, 9708−9719